RSC Advances

ROYAL SOCIETY OF CHEMISTRY

www.rsc.org/advances

Cite this: DOI: 10.1039/c0xx00000x

www.rsc.org/xxxxxx

ARTICLE TYPE

Hierarchical Core/Shell Structures of ZnO Nanorod@$CoMoO_4$ Nanoplates Used as a High-Performance Electrode for Supercapacitors

Yunjiu Cao,[ab] Lei An,[a] Lijun Liao,[a] Xijian Liu,[ab] Tao Ji,[ab] Rujia Zou,[a] Jianmao Yang,*[a] Zongyi Qin*[a] and Junqing Hu*[a]

Received (in XXX, XXX) Xth XXXXXXXXX 20XX, Accepted Xth XXXXXXXXX 20XX
DOI: 10.1039/b000000x

Hierarchical core/shell structures of ZnO nanorod@$CoMoO_4$ nanoplates grown directly on Ni foam were synthesized by a two-step hydrothermal process, in which ZnO nanorod arrays were first grown on Ni foam substrate, and then $CoMoO_4$ nanoplates were grown in multidirection on each ZnO nanorod. As-grown ZnO@$CoMoO_4$ core/shell structures (on Ni foam) directly used as integrated electrodes for electrochemical capacitors demonstrated prominent electrochemical performances, i. e., a high specific capacitance of 1.52 F cm^{-2} at a current density of 2 mA cm^{-2}, which was higher than that (772 mF cm^{-2}) of the pure $CoMoO_4$ electrode, and a good long-term cycling stability, which the electrodes retained 109% of the initial capacitance after 5000 cycles at a scan rate of 50 mV s^{-1}. The superior electrochemical performances suggest that the ZnO@$CoMoO_4$ core/shell structures could be considered as a prospective electrode material for the supercapacitors.

1. Introduction

Supercapacitors (SCs) may be one of most efficient storage energy devices in addressing the problems of climate change and the limited availability of fossils fuels in future. Compared to secondary batteries and conventional dielectric capacitors, supercapacitors have been paid considerable attention over the past decade due to high power density, fast charging/discharging characteristics and long cycle life.[1-5]

Electrode materials as a key part of supercapacitors can be classified as three kinds: carbonaceous materials,[6,7] transition metal oxides/hydroxides,[8,9] and conducting polymers.[10,11] Carbon-based materials absorb charge electrostatically at the electrode/electrolyte interface, leading to high power density at the cost of low energy density. By comparison, metal oxides/hydroxides and conducting polymers store charge by a faradaic or redox-type reaction similar to batteries, which enable high energy density. However, mechanical degradation of the conducting polymers due to the collapse of the polymer backbone during a limited number of charge-discharge process may lead to worse electrochemical performance and the metal oxide/hydroxide materials are not feasible application due to their poor electronic/ionic conductivity. Recently, composite pseudocapacitive transition metal oxides, such as $MnMoO_4$, $NiMoO_4$, $CoMoO_4$,[12-17] have been used as electrode materials, because they can supply different oxidation states for efficient redox reaction, which can obtain much higher specific capacitance and energy density.

Particularly, the $CoMoO_4$ has been investigated as one of the most promising electrode materials owing to the low cost, non-toxic, and enhanced electrochemical properties.[18-19] Xia et al. reported the $CoMoO_4$ nanoparticles with a specific capacitance of 72 F g^{-1}.[20] Such a low capacitance may result from the poor electronic conductivity of metal oxides, and thus largely limits their practical utilization. Recently, the rational design and synthesis of unique core/shell heterostructures have been identified to be an effective means to achieve enhanced electrochemical properties.[21-23] Mai et al. reported an improved the specific capacitance to 187 F g^{-1} from hierarchical structures of $MnMoO_4$/$CoMoO_4$ core/shell nanowires.[13] Recent studies by other groups also demonstrated that NiO@$CoMoO_4$ nanocomposites have a higher specific capacitance than pure $CoMoO_4$.[24] ZnO nanorod arrays have been extensively studied as a conductive support material due to their unique structure and properties, such as relatively good electrical conductivity, which provides a natural pathway for electron transport.[25-27] In this regard, various core/shell nanostructures such as ZnO@Co_3O_4,[28] ZnO@MoO_3,[29] ZnO@NiO/MoO_2,[30] have been fabricated and demonstrated their improved electrochemical performances. Therefore, $CoMoO_4$ electrode materials supported with ZnO nanorod substrate can increase the electrical conductivity and enhance the electrochemical performance.

In this work, we have prepared hierarchical core/shell structures of ZnO nanorod@ $CoMoO_4$ nanoplates (ZnO @$CoMoO_4$) on Ni foam for their supercapacitor applications via a two-step hydrothermal process followed by a calcination treatment. ZnO@$CoMoO_4$ core/shell electrode materials not only retain the advantages of $CoMoO_4$, such as the multiple valence states, environmentally benign nature, affordable cost, and natural abundance, but also improve the electron conductivity of the overall electrode. Meanwhile, the ZnO nanorod arrays serve as a scaffold, providing large surface area for the growth of $CoMoO_4$

nanoplates. Moreover, the $CoMoO_4$ nanoplates with large specific surface area can be beneficial for the improvement of areal specific capacitance. The ZnO nanorod arrays could also prevent the conventional aggregation of active materials that degrade the cycle stability. Here, this hierarchical core/shell structures of ZnO@$CoMoO_4$ exhibits a high areal specific capacitance of 1.52 F cm^{-2} (1169 F g^{-1}) at the current density of 2 mA cm^{-2}, and an excellent cycle stability with 109% retention after 5000 cycles at a scan rate of 50 mV s^{-1}. Thus, these hierarchical ZnO@$CoMoO_4$ core/shell structures can be expected to be a promising candidate for supercapacitor applications.

2. Experimental Section

2.1 Preparation of ZnO nanorod arrays on Ni Foam

In this experiment, all the chemicals were analytical grade and were used without further purification. Ahead of the experiment, the Ni foam substrate (1 × 1 cm^2) was ultrasonically washed with ethanol and water for 20 min each and then soaked in 0.5M $KMnO_4$ for 30 min to form a seed layer. The reaction solution was prepared by mixing 0.015 M zinc nitrate hexahydrate and 0.015 M hexamethylenetetraamine (HMTA) together with 4 mL of ammonia in 100 mL of distilled water under constant magnetic stirring for 30 min. The Ni foam substrate was then dipped into the reaction solution and kept at 90 °C for 24 h. After the reaction, the Ni foam coated with white products was washed with deionized water, and thus the ZnO nanorods were obtained.

2.2 Preparation of ZnO nanorod@$CoMoO_4$ nanoplates

The ZnO nanorods prepared as described above were used as the scaffold for the growth of $CoMoO_4$ via a facile hydrothermal method. First, 1 mmol of $CoCl_2 \cdot 6H_2O$ and 1mmol of $Na_2MoO_4 \cdot 7H_2O$ were dissolved in 50 mL of distilled water under constant magnetic stirring for 30 min. Second, the above solution was transferred into autoclave liner, and the as-prepared ZnO nanorods (substrate) was immersed into the reaction solution. Finally, the solution was sealed in a stainless steel autoclave and maintained at 150 °C for 5 h. After the reaction, in order to remove the residuals, the Ni foam substrate with light pink color was washed with deionized water for a few minutes and then dried at 60 °C for 12 h. Afterward, the sample was annealed at 300 °C for 2 h in air, and thus the ZnO nanorod@$CoMoO_4$ nanoplates were obtained. For comparison, we also prepared pure $CoMoO_4$ (without a ZnO nanorod) using the same method under the same conditions.

2.3 Materials characterization

The morphology and microstructure of electrode materials were characterized using a scanning electron microscopy (SEM; S-4800) and a transmission electron microscopy (TEM; JEM-2100F) equipped with an energy dispersive spectrometer (EDS). The synthesized samples were characterized with a D/max-2550 PC X-ray diffractometer (XRD; Rigaku, Cu-Kα radiation). The mass of electrode materials was weighed on a XS analytical balance (Mettler Toledo; δ = 0.01 mg).

2.4 Electrochemical Characterizations

Electrochemical properties of ZnO@$CoMoO_4$ core/shell structure materials were studied with cyclic voltammetry (CV), charge−discharge measurements, and electrochemical impedance spectroscopy (EIS) tests in an electrochemical workstation (Autolab PGSTAT302N potentiostat) using a three-electrode electrochemical configuration in 1 M KOH aqueous solution. The ZnO@$CoMoO_4$ core/shell structure materials (1 × 1 cm^2, the mass of ZnO nanorods and $CoMoO_4$ nanoplates of ~ 2 mg and 1.3 mg, respectively) were directly used as the working electrode. A platinum electrode was used as counter electrode, and a saturated calomel electrode was used as reference electrode. The pure $CoMoO_4$ (~ 1.5 mg cm^{-2}) was also tested with electrochemical properties for comparison.

3. Results and Discussion

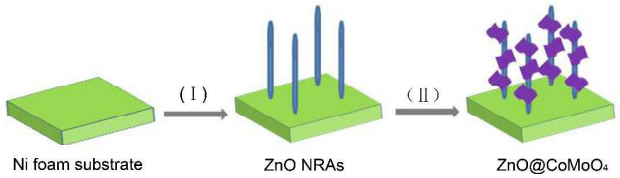

Fig. 1 Schematic illustration of the formation process of ZnO@$CoMoO_4$ hierarchical core/shell heterostructure.

Fig. 1 illustrates the two-step synthesis of the ZnO/$CoMoO_4$ core/shell heterostructure via hydrothermal process. First ZnO nanorod array is grown on Ni foam substrate. And then the as prepared ZnO nanorod arrays on Ni foam is subsequently coated by multidirectional and interconnected $CoMoO_4$ nanoplates.

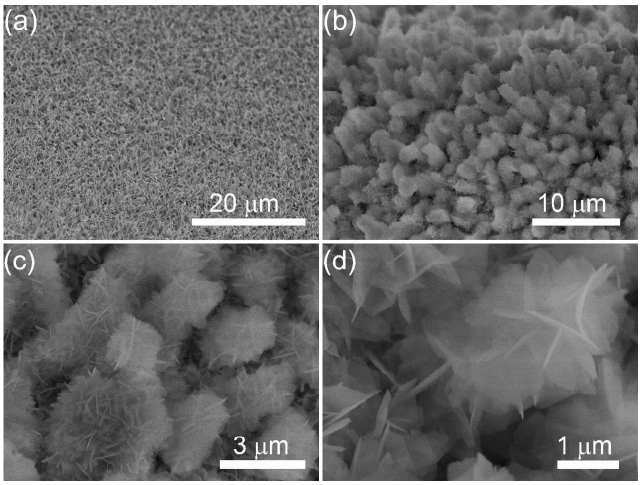

Fig. 2 (a) The low magnification SEM images of ZnO nanorods. (b-d) Low and high magnification SEM images of ZnO@$CoMoO_4$ core/shell heterostructures grown directly on Ni foam.

The morphology of the ZnO@$CoMoO_4$ core/shell heterostructures on Ni foam was first analyzed by SEM. Fig. 2 a demonstrates the growth of ZnO nanorods on Ni foam. It can be clearly seen that ZnO nanorods was uniformly grown on Ni foam. The diameter and length of ZnO nanorods are about 250 nm and 6 μm, respectively (see Supporting Information, Fig. S1). The Ni foam is uniformly covered by ZnO@$CoMoO_4$ core/shell heterostructures at a large scale, as shown Fig. 2b and 2c. It can be also seen from the high magnification images (Fig. 2d) that ZnO nanorods are uniformly coated by $CoMoO_4$ nanoplates. The

$CoMoO_4$ nanoplates are firmly interconnected with each other to form some gaps betweem them on surface of ZnO nanorods. Further insight into the ZnO@$CoMoO_4$ core/shell structures were provided by TEM studies. As shown in Fig. 3 a, b the core/shell structure is easily observed from an individual ZnO@$CoMoO_4$ core/shell structure, where the ZnO core is covered by $CoMoO_4$ nanoplates. The HRTEM image of the $CoMoO_4$ nanoplate shown in the insert of Fig. 3b displays an interplanar spacing of 0.244 nm, corresponding to the (400) plane of the $CoMoO_4$.

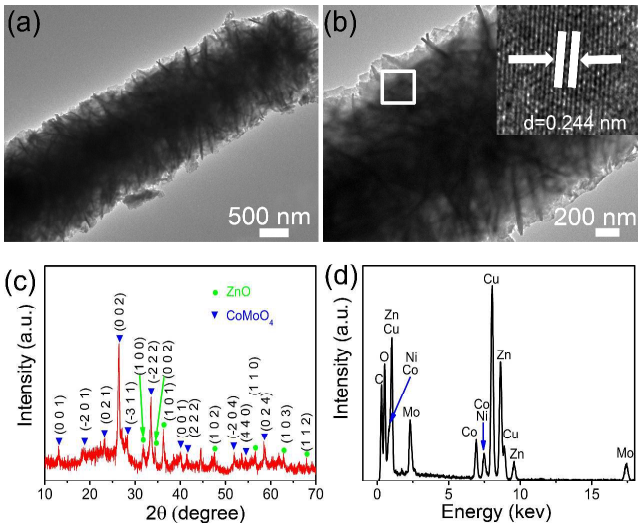

Fig. 3 TEM (a) and high-resolution TEM (b) images of an individual ZnO@$CoMoO_4$ core/shell structure. (c) Typical XRD pattern of ZnO@$CoMoO_4$ core/shell structures scratched from the Ni foam. (d) EDS pattern of ZnO@$CoMoO_4$ core/shell structure

XRD analysis was employed to further investigate the crystal structure and phase composition, as shown in Fig. 3c. The ZnO@$CoMoO_4$ core/shell structures were scratched from Ni foam in order to avoid the strong peaks from the Ni foam substrate. It is obvious that the diffraction signal of the powders can be indexed to the standard diffraction patterns of ZnO (JCPDS no. 79-2205) and $CoMoO_4$ (JCPDS No. 21-0868). The energy dispersive spectrometry (EDS) was carried out in TEM to further verify the elemental composition of the individual ZnO@$CoMoO_4$ core/shell structures. The EDS result reveals the presence of elements of Zn, Co, Mo and O, as shown in Fig. 3d.

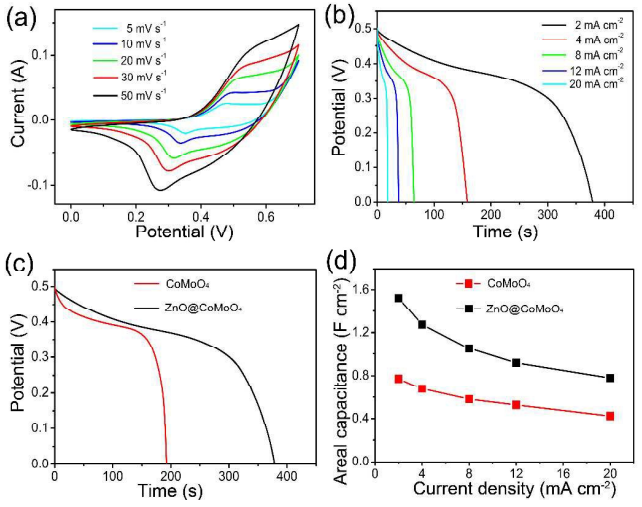

Fig. 4 (a) CV curves of the ZnO@$CoMoO_4$ core/shell hierarchical electrode at various scan rates. (b) Galvanostatic discharge curves of the ZnO@$CoMoO_4$ on Ni foam electrode at various current densities. (c) A comparison of Galvanostatic discharge curves of the ZnO@$CoMoO_4$ and pure $CoMoO_4$ electrodes at discharge current densities of 2 mA cm^{-2}. (d) A comparison of specific capacitances for the ZnO@$CoMoO_4$ and pure $CoMoO_4$ as a function of current density.

The obtained ZnO@$CoMoO_4$ core/shell heterostructures on Ni foam were directly used as binder-free electrodes for the electrochemical performance evaluation. The electrochemical measurements were carried out in a three- electrode system with a 1 M KOH aqueous solution as electrolyte. The cyclic voltammogram (CV) curves of the ZnO@$CoMoO_4$ electrodes were recorded at various scan rates within the potential range of 0 to 0.7 V as shown in Fig. 4a. A pair of redox peaks observed in all the CV curves is apparently different from the CV curves of electric double layer capacitors (EDLCs) that are similar to an ideal rectangular shape, indicating that the electrochemical performance of electrodes results from the pseudocapacitive capacitance.[31,32] As the scan rates increases, the oxidation and reduction peaks shift to higher and lower potential, respectively, which could be attributed to the internal resistance of the electrode. Fig. S2 (see Supporting Information) shows the CV comparison of the ZnO@$CoMoO_4$ and $CoMoO_4$ electrodes recorded at the scan rate of 50 mV s^{-1}. The CV curve integral area of the ZnO@$CoMoO_4$ electrode is much larger than that of $CoMoO_4$ electrode. It suggests that the ZnO nanorods used as conductive support for $CoMoO_4$ material can greatly enhance electrochemical performance of $CoMoO_4$ material.

Galvanostatic charge-discharge measurements were performed at various currents from 2 mA cm^{-2} to 20 mA cm^{-2}. The typical discharge curves of the ZnO@ $CoMoO_4$ electrodes at different current densities within the potential window of 0−0.5 V are presented in Fig. 4b. The areal capacitance for the ZnO@$CoMoO_4$ electrodes can be calculated based on the discharge curves. There is a distinct plateau region in each discharge process, indicating that the capacitance derives from redox reaction, which is consistent with the CV curves. By comparison, Fig. 4c shows the discharge profiles of the ZnO@$CoMoO_4$ electrodes and the pure $CoMoO_4$ electrode at 2 mA cm^{-2}. As can be seen, the discharge time of ZnO@$CoMoO_4$ electrodes is much longer than that the pure $CoMoO_4$ electrode, which indicates that ZnO@$CoMoO_4$ electrodes exhibits a higher areal specific capacitance. The calculated results are displayed in Fig. 4d. The ZnO@$CoMoO_4$ electrode displays high areal capacitance values of 1.52, 1.27, 1.05, 0.92 and 0.78 F cm^{-2} at different current densities of 2, 4, 8, 12 and 20 mA cm^{-2}, respectively. The capacitance can retain 51.3% of its initial value even if the current density increases by 10 times, indicating a good rate capability. However the pure $CoMoO_4$ electrode exhibits lower areal capacitance values of 772, 678, 581, 528 and 424 mF cm^{-2} at the same current densities. It is obvious that ZnO@$CoMoO_4$ electrode delivers higher areal specific capacitance than the pure $CoMoO_4$ electrode. The result may be attributed to the special role of the ZnO nanorod arrays within these core/shell structure providing a large surface area for the growth of $CoMoO_4$ nanoplates which thus improved the surface area of active materials and avoided the conventional aggregation of the active materials. Furthermore, the capacitance of the

$ZnO@CoMoO_4$ electrode is also superior to previously reported $CoMoO_4$ electrodes, such as $CoMoO_4 \cdot 0.9H_2O$ nanorods (326 F g^{-1} at 5 mA cm^{-2}),[33] $CoMoO_4$ nanorods (286 F g^{-1} at 5mA cm^{-2}),[34] $MnMoO_4/CoMoO_4$ heterostructured nanowires (187.1 F g^{-1} at 1 A g^{-1}),[13] porous ZnO/NiO composite micropolyhedrons (649 F g^{-1} at 5.8 A g^{-1}),[35] and Co_3O_4/NiO core/shell nanowire arrays (452 F g^{-1} at 2 A g^{-1}). [22]

The long-term cycling stability of electrodes is also an important requirement for practical supercapacitor applications. The electrochemical stability of the $ZnO@CoMoO_4$ core/shell electrode is evaluated by repeated CV processes at a scan rate of 50 mV s^{-1} for 5000 cycles as shown in Fig. 5a. The CV curves before and after cycling are displayed in Fig.S3, where integral area of the 5000th cycle was larger than that of the first cycle. It is observed that the cycle stability is greatly enhanced in the $ZnO@CoMoO_4$ electrode and maintains 109% of its initial value after 5000 cycles. The possible explanation is that only a part of electrode material is active at first. More and more sites become activated and contribute to the capacitance increasing as the electrolyte gradually penetrates into the inner region of the electrode.[36] Moreover, the ZnO nanorods possess the chemical stability and are tightly integrated with the $CoMoO_4$, making the structure stable and strengthening the structural integrity of the core during the charge-discharge process, resulting in enhanced cycle stability. This result shows that the combination of complex metal oxide ($CoMoO_4$) nanoplates with ZnO nanorods provides high electrochemical stability for long cycle life applications.[37, 38]

The electrochemical impedance spectroscopy measurements were further employed to discuss the electrochemical behavior of the $ZnO@CoMoO_4$ electrode before and after cycling. The corresponding Nyquist plots were shown at Fig. 5b. The internal resistance of the electrochemical system (Rs) can be estimated from the intercept of the curve at Z'-axis at the high frequency, which includes the intrinsic resistance of the substrate, ionic resistance of electrolyte and contact resistance between current collector and active material. Warburg resistance (W) is estimated by the slope of the linear portion of the curve on the right of the semicircle, which is a result of the frequency dependent ion diffusion/transport in the electrolyte toward the electrode surface. It can be seen that both Rs and W of the $ZnO@CoMoO_4$ electrode exhibit subtle changes after a long time cycling, indicating that the 3D structure of the $ZnO@CoMoO_4$ was favorable for the penetration of the electrolyte within the electrode, the enhanced utilization of the electrode materials, and higher areal specific capacitance value, which can well explain the increase of the capacitance as described above.

The high areal specific capacitance, good rate capability, and excellent cycle stability of the $ZnO@CoMoO_4$ could be attributed to the following factors: First, the 3D structure of ZnO nanorod arrays acted as a scaffold, providing a large surface area for the growth of the $ZnO@CoMoO_4$ and accelerating electron transport for the Faradaic reaction. Second, the gaps between the neighboring $ZnO@CoMoO_4$ made the electrolyte fully penetrate into the inner region of the electrode, facilitating the transport of the electrolyte and ensuring efficient contact between the electrode material and the electrolyte, thus increasing the utilization of the active materials. Third, the $ZnO@CoMoO_4$ core/shell structures were directly grown on the current collector (Ni foam), avoiding the use of polymer binders and conducting additives, which improves the utilization of the electrode material. Most importantly, the ZnO nanorods were grown directly on the Ni foam (substrate) with a robust adhesion and bridged the $CoMoO_4$ nanoplates with the current collector, which can facilitate electron transport during the processes of charging and discharging because of its high electrical conductivity.

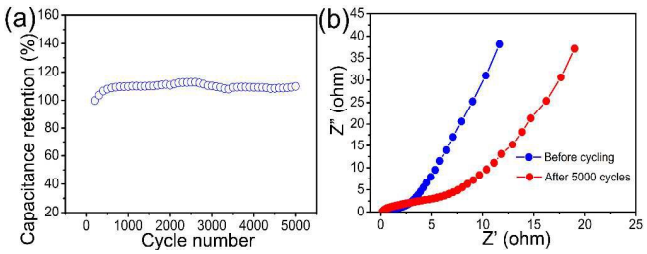

Fig. 5 (a) Cycling performance of the $ZnO@CoMoO_4$ core/shell structure on Ni foam at a scan rate of 50 mV s^{-1}. (b) Electrochemical impedance spectra before and after cycling.

4. Conclusions

In sum, we have adopted a two step hydrothermal method to synthesize hierarchical core/shell $ZnO@CoMoO_4$ nanostructures on the 3D continuous porous Ni foam and used these nanostructures as high performance electrochemical capacitor electrode. The electrochemical examinations show that as-fabricated electrodes made of such a nanomaterial possessed a high area specific capacitance of 1.57 F cm^{-2} (1169 F g^{-1}) at the current density of 2 mA cm^{-2} and a good cycling stability of 109% of the initial specific capacitance after the 5000 repetitive cycle processes. These results suggest that such architecture is a promising electrode material for high-performance electrochemical capacitor.

Acknowledgements

This work was financially supported by the National Natural Science Foundation of China (Grant No. 21171035 and 51272299), the Key Grant Project of Chinese Ministry of Education (Grant No. 313015), the Scientific Research Foundation for the Returned Overseas Chinese Scholars, the Science and Technology Commission of Shanghai-based "Innovation Action Plan" Project (Grant No. 10JC1400100), Shanghai Rising-Star Program (Grant No. 11QA1400100), Innovation Program of Shanghai Municipal Education Commission (Grant No. 13ZZ053), Shanghai Leading Academic Discipline Project (Grant No. B603), Ph.D. Programs Foundation of Ministry of Education of China (Grant No. 20110075110008), the Fundamental Research Funds for the Central Universities, and the Program of Introducing Talents of Discipline to Universities (Grant No. 111-2-04).

Notes and references

[a]*State Key Laboratory for Modification of Chemical Fibers and Polymer Materials, College of Materials Science and Engineering, Donghua University, Shanghai 201620, China.*
[b]*School of Fundamental Studies, Shanghai University of Engineering Science, Shanghai 201620, China*

Cite this: DOI: 10.1039/c0xx00000x

www.rsc.org/xxxxxx

ARTICLE TYPE

Fax: +86-21-6779-2947; Tel: +86-21-6779-2947; E-mail: yangjm@dhu.edu.cn; phqin@dhu.edu.cn;hu.junqing@dhu.edu.cn;

†Electronic Supplementary Information (ESI) available: [Experimental process, Supplementary Fig.s and Specific capacitance calculation].

See DOI: 10.1039/b000000x/

1. J. R. Miller and P. Simon, *Science*, **2008**, *321*, 651.
2. P. Simon and Y. Gogotsi, *Nat. Mater.*, **2008**, *7*, 845.
3. Y. Sun , Q. Wu , G. Shi , Energy Environ. Sci., 2**011** , *4* , 1113 .
4. X. Yu, B. Lu, Z. Xu, *Adv. Mater.,* **2014** , *26* , 1044 .
5. Y. Huang , J. Liang , Y. Chen , *Small*, **2012** , *8* , 1805 .
6. Y. Zhu, S. Murali, M. D. Stoller, K. J. Ganesh, W. Cai, P. J. Ferreira, A. Pirkle, R. M. Wallace, K. A. Cychosz, M. Thommes, D. Su, E. A. Stach and R. S. Ruoff, *Science*, **2011**, *332*, 1537.
7. A. B. Fuertes and M. Sevilla, *ACS Appl. Mater. Interfaces*, **2015**, *7*, 4344.
8. C. H.Tang, Z. Tang, H. Gong, J. Electrochem. Soc., 2012, 159, A651.
9. Y. J. Zhang, C. T. Sun, P. Lu, K. Y. Li, S. Y. Song, D. F. Xue, *CrystEngComm.*, **2012**, *14*, 5892.
10. K. Zhang, L. L. Zhang, X. S. Zhao, J. Wu, *Chem. Mater.*, **2010**, *22*, 1392.
11. A. Bahloul, B. Nessark, E. Briot, H. Groult, A. Mauger, K. Zaghib, C. M. Julien, *J. Power Sources*, **2013**, *240*, 267.
12. K. K. Purushothaman, M. Cuba and G. Muralidharan, *Mater. Res. Bull.*, **2012**, *47*, 3348.
13. L. Q. Mai, F. Yang, Y. L. Zhao, X. Xu, L. Xu and Y. Z. Luo, *Nat. Commun.*, **2011**, *2*, 381.
14. M. C. Liu, L. Kang, L. B. Kong, C. Lu, X. J. Ma, X. M. Lia and Y. C. Luo, *RSC Adv.*, **2013**, *3*, 6472.
15. B. Senthilkumar, K. V. Sankar, R. K. Selvan, M. Danielleb and M. Manickamb, *RSC Adv.*, **2013**, *3*, 352.
16. G. K. Veerasubramani, K. Krishnamoorthy, S. Radhakrishnan, N. J. Kim, S. J. Kim, *Int J Hydrogen energ.*, **2014**, *39*, 5186.
17. Z. Xu, Z. Li, X. Tan, C. M. B. Holt, L. Zhang, B. S. Amirkhiz and D. Mitlin, *RSC Adv.*, **2012**, *2*, 2753.
18. Y. Ding, Y. Wan, L. Min, W. Zhang, S. H. Yu, *Inorg Chem.*, **2008**, *47*, 7813.
19. J. Zhao, Q. S. Wu, M. Wen, *J Mater Sci.*, **2009**, *44*, 6356.
20. X. Xia, W. Lei, L. Hao, W. Wang, X. Wang, *Electrochim. Acta*, **2013**, *99*, 253.
21. X. Xia, J. Tu, Y. Zhang, X. Wang, C. Gu, X. Zhao, H. J. Fan, *ACS Nano*, **2012**, *6*, 5531.
22. C. Zhou, Y. Zhang, Y. Li, J. Liu, *Nano Lett.*, **2013**, *13*, 2078.
23. X. Y. Xue, Z. H. Chen, L. L. Xing, S.Yuan, Y. J. Chen, *Chem. Commun.*, **2011**, *47*, 5205.
24. X. J. Ma, L. B. Kong, W. B. Zhang, M.C. Liu, Y. C. Luo and L. Kang, *RSC Adv.*, **2014**, *4*, 17884.
25. J. Liu, X. Huang, Y. Li, X. Ji, Z. Li, X. He and F. Sun, *J. Phys.Chem. C*, **2007**, *111*, 4990.
26. H. J. Fan, P. Werner and M. Zacharias, *Small*, **2006**, *2*, 700.
27. J. Jiang, Y. Li, J. Liu and X. Huang, *Nanoscale*, **2011**, *3*, 45.
28. X. Xia, J. Tu, Y. Zhang, X. Wang, C. Gu, X.B. Zhao and H. J. Fan, *ACS Nano*, **2012**, *6*, 5531.
29. G. R. Li, Z. L. Wang, F. L. Zheng, Y. N. Ou and Y. X. Tong, *J. Mater. Chem.*, **2011**, *21*, 4217.
30. S. C. Hou, G. H. Zhang, W. Zeng, J. Zhu, F. L. Gong, F. Li, and H. G. Duan, *ACS Appl. Mater. Interfaces*, **2014**, *6*, 13564.
31. C. Yuan, L.Yang, L. Hou, L. Shen, X. Zhang, X. W. Lou, *Energy Environ. Sci.*, **2012**, *5*, 7883.
32. G. Q. Zhang, H. B. Wu, H. E. Hoster, M. B. Chan Park, X. W. Lou, *Energy Environ. Sci.*, **2012**, *5*, 9453.
33. M. C. Liu, L. B. Kong, X. J. Ma, C. Lu, X. M. Li, Y. C. Luo and L. Kang, *New J. Chem.*, **2012**, *36*, 1713.
34. C. Z. Yuan, L. Yang, L. R. Hou, J. Y. Li, Y. X. Sun, X. G. Zhang, L. F. Shen, X. J. Lu, S. L. Xiong and X. W. Lou, *Adv. Funct. Mater.*, **2012**, *22*, 2560.
35. H. Pang, Y. H. Ma, G. C. Li, J. Chen, J. S. Zhang, H. H. Zheng, W. M. Du, *Dalton Trans.*, **2012**, *41*, 13284.
36. X. Y. Liu, Y. Q. Zhang, X. H. Xia, S. J. Shi, Y. Lu, X. L. Wang, C. D. Gu, J. P. Tu, *J. Power Sources*, **2013**, *239*, 157.
37. Z. Xing, Q. Chu, X. Ren, C. Ge, A. H. Qusti, A. M. Asiri, A. O. Al-Youbi, X. Sun, *J. Power Sources*, **2014**, *245*, 463.
38. Z. Pu, Q. Liu, A. H. Qusti, A. M. Asiri, A. O. Al-Youbi, X. Sun, *Electrochim. Acta*, **2013**, *109*, 252.

The table of contents entry

$ZnO@CoMoO_4$ hierarchical core/shell structures for high-performance supercapacitors were synthesized by two facile hydrothermal process and exhibited a high specific capacitance of 1.52 F cm^{-2} (1169 F g^{-1}) at 2 mA cm^{-2} and a good cycling stability of 109% of the initial specific capacitance after 5000 cycles.